Field Induced Multiple Superconducting Phases in UTe_2 along Hard Magnetic Axis

H. Sakai,[1,*] Y. Tokiwa,[1] P. Opletal,[1] M. Kimata,[2] S. Awaji,[3] T. Sasaki,[2] D. Aoki,[4] S. Kambe,[1] Y. Tokunaga,[1] and Y. Haga[1]

[1]*Advanced Science Research Center, Japan Atomic Energy Agency, Tokai, Ibaraki 319-1195, Japan*
[2]*Institute for Materials Research, Tohoku University, Sendai, 980-8577, Japan*
[3]*High Field Laboratory for Superconducting Materials, Institute for Materials Research, Tohoku University, Sendai 980-8577, Japan*
[4]*Institute for Materials Research, Tohoku University, Oarai, Ibaraki 311-1313, Japan*

(Received 3 October 2022; revised 19 December 2022; accepted 4 April 2023; published 12 May 2023)

The superconducting (SC) phase diagram in uranium ditelluride is explored under magnetic fields (H) along the hard magnetic b axis using a high-quality single crystal with $T_c = 2.1$ K. Simultaneous electrical resistivity and ac magnetic susceptibility measurements discern low- and high-field SC (LFSC and HFSC, respectively) phases with contrasting field-angular dependence. Crystal quality increases the upper critical field of the LFSC phase, but the H^* of ∼15 T, at which the HFSC phase appears, is always the same through the various crystals. A phase boundary signature is also observed inside the LFSC phase near H^*, indicating an intermediate SC phase characterized by small flux pinning forces.

DOI: 10.1103/PhysRevLett.130.196002

Uranium ditelluride (UTe_2) has attracted considerable attention as a strong candidate for spin-triplet and topological superconductivity. Ran *et al.* [1] initially reported unconventional superconductivity of this compound with a superconducting (SC) transition temperature (T_c) of 1.6 K and vast upper critical field (H_{c2}) that exceeds the Pauli-limiting field. Slight decreases in the nuclear magnetic resonance (NMR) shift strongly suggest the spin-triplet SC pairing under ambient pressure [2–4]. Meanwhile, the discovery of multiple SC phases under pressure further supports spin-triplet formation with spin degrees of freedom [5–8]. The topological aspect of the SC state is experimentally suggested through scanning tunneling microscopy [9], polar Kerr effect [10], and London penetration depth [11] measurements.

UTe_2 crystallizes in a body-centered orthorhombic structure ($Immm$) [12,13]. Magnetic-field-reinforced superconductivity, an extraordinary phenomenon in UTe_2, appears when a magnetic field (H) is applied along the crystallographic b axis, which is perpendicular to the easy magnetic a axis, along which uranium $5f$ spin moments favor aligning with an Ising character [14–18]. In $H \| b$, T_c initially decreases with increasing H, and then starts to increase above $\mu_0 H^* \simeq 15$ T, i.e., a characteristic ⊥ shape $H_{c2}(T)$ appears. Superconductivity persists up to a metamagnetic transition at $\mu_0 H_m \simeq 34.5$ T and suddenly disappears above H_m.

Previously, one might assume a uniform SC state was realized in UTe_2 below the ⊥ shape $H_{c2}(T)$ because an internal transition could not be found. However, two discernible SC phases in the case of $H \| b$ are reported by specific heat measurement using a crystal with $T_c = 1.85$ K in the case of $H \| b$ [19], which is also detected by ac magnetic susceptibility (χ_{ac}) for a crystal of $T_c = 1.85$ K [20]. Remarkably, a second-order phase transition is observed inside the SC state, which separates the low- and high-field SC (LFSC and HFSC, respectively) phases with $\mu_0 H^* \simeq 15$ T. As a thermodynamic consideration [21], however, three second-order transition lines cannot meet at a single point unless another line emerges from here. These results motivate us to continue the studies using a higher-quality single crystal.

The SC properties of UTe_2 clearly depend on the sample quality. Since impurity effects are completely unknown in rare spin-triplet SC cases, it is exceptionally necessary to remove defects as much as possible. Although growth condition optimization using a chemical vapor transport (CVT) method increased T_c up to 2 K and the residual resistivity ratio (RRR) up to ∼88 [22,23], CVT crystals still contain a small number of uranium vacancies within 1%—even in high-T_c crystals [24,25]. Recently, UTe_2 crystals higher T_c of 2.1 K and larger RRRs far over 100 have been grown using the molten salt flux (MSF) method [26]. The detection of de Haas–van Alphen oscillations [27] guarantees these crystals of high quality with a long mean free path and lower impurity scatterings. So far, the other quantum oscillation experiments have only been reported on the MSF samples [28,29]. In this Letter, we explore the SC phase diagram of such an ultraclean UTe_2 crystal to search for a missing phase line inside the SC state. For this purpose, the electrical resistivity (ρ) and change of χ_{ac} were *in situ* measured simultaneously on an identical crystal.

Figure 1(a) schematically illustrates the experimental setup of this study. A crystal was selected with a size of $0.73 \times 0.75 \times 4.6$ mm^3 and RRR = 180. The crystal was mounted on a two-axis goniostage, and the probe was

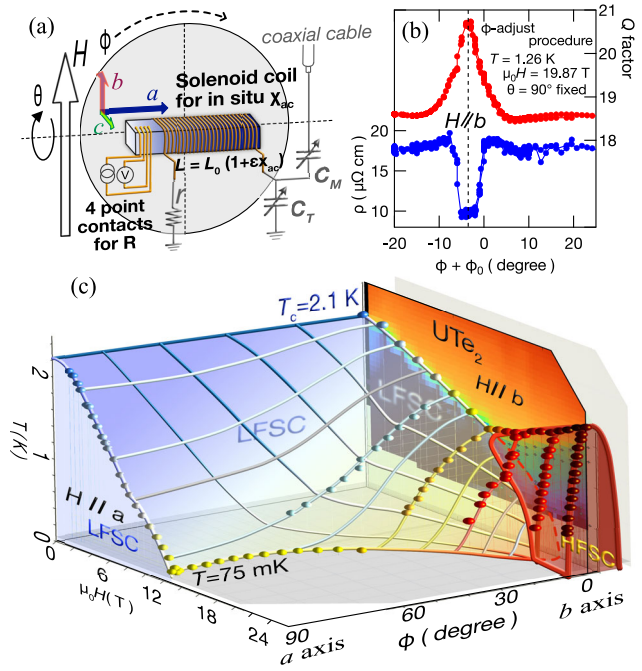

FIG. 1. (a) Schematic illustration of the simultaneous measurement of ρ and $\Delta\chi_{ac}$. The rf circuit comprises a solenoid coil filled with the sample and two variable capacitors at room temperature. The definitions of angles θ and ϕ with the external field (H) are also presented here. (b) ϕ rotation dependence of ρ and Q of the rf circuit with a fixed angle of $\theta = 90°$ ($H \perp c$). (c) Three-dimensional schematic plot on the angular dependence of the LFSC and HFSC phases from the b axis to the a axis for UTe_2.

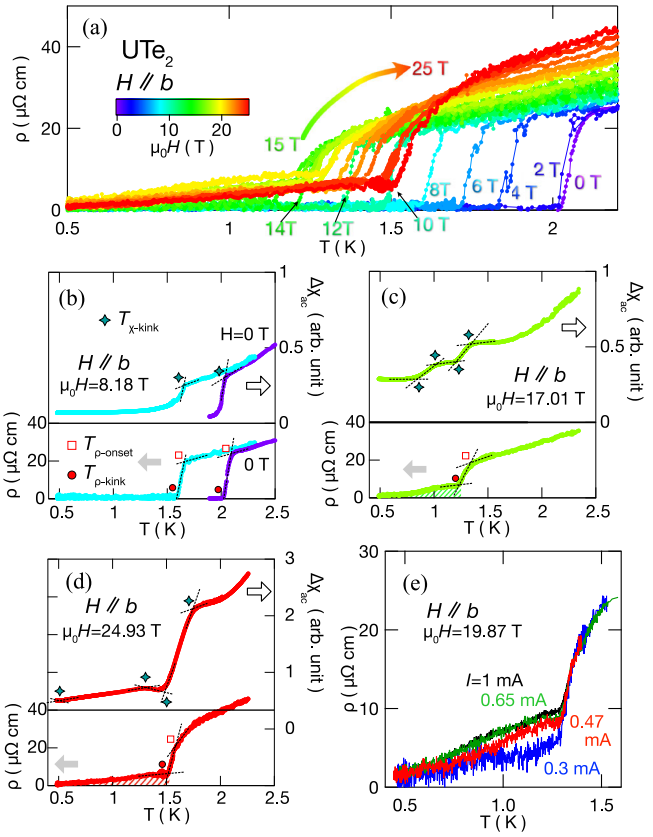

FIG. 2. (a) ρ vs T plots for various H applied along the b axis. Temperature dependence of ρ and $\Delta\chi_{ac}$ for (b) zero field and $\mu_0 H = 8.18$ T, (c) $\mu_0 H = 17.01$ T, and (d) $\mu_0 H = 24.93$ T applied along the b axis. Here, $\Delta\chi_{ac}$ is defined as $(\Delta\nu_{Tune})^{-2}$ with $\Delta\nu_{Tune} \equiv \{\nu_{Tune} - \nu_0\}/\nu_0$. The resonant frequency ν_0 was set to 3.7 MHz, and the matching for the rf circuit was adjusted at $T = 4.2$ K. (e) ρ vs T plots measured with several ac currents of $I_{ac} = 0.3$, 0.47, 0.65, and 1 mA for $\mu_0 H = 19.87$ T.

inserted into a ^{3}He cryostat. $\rho(T, H)$ was measured using the ac four-probe method with a current of 0.3 mA. The resonance frequency of the tank circuit $\nu_{Tune} = (2\pi\sqrt{LC})^{-1}$, where L and C are the inductance and capacitance, respectively, was measured by a vector network analyzer using a tiny rf field of a few μT. If χ_{ac} is reduced due to SC diamagnetism, $L = L_0(1 + \epsilon\chi_{ac})$ decreases, where ϵ is a filling factor of the sample to the coil. Consequently, the onset T_c was detected as a kink in $\Delta\nu_{Tune} = (\nu_{Tune} - \nu_0)/\nu_0 \propto 1/\sqrt{\Delta\chi_{ac}}$. Here, we set $\nu_0 \simeq 3.7$ MHz by tuning the variable capacitors shown in Fig. 1(a), which were fixed during measurements. External fields were applied using a 25 T cryogen-free SC magnet in the High Field Laboratory for Superconducting Materials (HFLSM), Institute for Materials Research (IMR), Tohoku University. We could precisely adjust the H orientation along the crystal b axis by monitoring ρ and the quality factor (Q) of the rf circuit by rotating the goniostage, as shown in Fig. 1(b), where Q is proportional to $\sqrt{L/C}$.

In this study, the distinction between the LFSC and HFSC phases was observed based on their H orientation dependence, which is summarized as a three-dimensional phase diagram in Fig. 1(c). To determine T_c of each phase, the kink of $\Delta\nu_{Tune}(\phi)$ is tracked by rotating the field angle ϕ from the b and a directions (see the Supplemental Material [30]). As also shown in this figure, the HFSC phase is rapidly suppressed when H is turned away from the b direction, whereas the LFSC phase is much more robust to the ϕ. The strong ϕ dependence of the HFSC state is consistent with that of a previous study on CVT-grown crystals [15]. The narrow field-angle HFSC phase is also observed in ferromagnetic (FM) superconductors UCoGe and URhGe when the field is rotated around the magnetically hard axis [31,32]. For these FM superconductors, the behavior is considered a consequence of H induced suppression of Ising-type, longitudinal FM spin fluctuations, as detected by NMR [33,34]. However, this longitudinal mode of fluctuations in the high H has not been confirmed yet in UTe_2.

Hereafter, we focus on the experiments of applying H along the b axis. Figure 2(a) shows the T dependence of $\rho(T)$ at various H along the b axis (also see the Supplemental Material [30]). The change of ac magnetic susceptibility is defined as $\Delta\chi_{ac} \equiv (\Delta\nu_{Tune})^{-2}$. The results

of simultaneous $\Delta\chi_{\rm ac}(T)$ measurements are presented in the Supplemental Material [30]. At zero field, as shown in Figs. 2(a) and 2(b), $\rho(T)$ drops at $T_{\rho\,\rm onset} = 2.1$ K and becomes zero below $T_{\rho\,\rm kink} = 2.02$ K. $\Delta\chi_{\rm ac}$ also exhibits a kink at the same temperature (denoted as $T_{\chi\,\rm kink}$). Similarly, we can recognize related anomalies that correspond to $T_{\rho\,\rm onset}$, $T_{\rho\,\rm kink}$, and $T_{\chi\,\rm kink}$ for the data in $\mu_0 H_0 = 8.18$ T.

As for the data in $\mu_0 H = 17.01$ T, we can still recognize anomalies for $T_{\rho\,\rm onset} = 1.31$ K and $T_{\rho\,\rm kink} = 1.23$ K. Meanwhile, the anomaly in $\rho(T)$ at $T_{\rho\,\rm onset}$ is no longer a distinct kink but becomes a shoulderlike bend. Notably, the value of $\rho(T)$ remains finite below $T_{\rho\,\rm kink}$. As the T is further lowered, $\rho(T)$ gradually decreases and finally drops to zero at T of ~0.5 K. In Figs. 2(c) and 2(d), we hatch the area where $\rho(T)$ is finite below $T_{\rho\rm kink}$. The finite $\rho(T)$ is attributed to the so-called flux-flow resistivity, which is also supported by the current (I) dependence of ρ, as shown in Fig. 2(e). Notably, this flux-flow resistivity appears only above $\mu_0 H \simeq 15$ T, as shown in Fig. 2(a) (also see the Supplemental Material [30]). In high fields, $\Delta\chi_{\rm ac}$ bends slightly above $T_{\rho\,\rm onset}$ and multiple kinks are observed as T is further lowered [e.g., see Fig. 2(c)]. In $\mu_0 H = 24.93$ T, as shown in Fig. 2(d), the first kink of $\Delta\chi_{\rm ac}$ appears at $T_{\chi\,\rm kink} = 1.72$ K higher than $T_{\rho\,\rm onset} = 1.57$ K, and then multiple kinks appear at lower temperatures.

Subsequently, let us turn to H scans along the b axis. Figure 3 shows the H dependence of ρ and $\Delta\chi_{\rm ac}$ at $T = 0.49$, 1.0, and 1.3 K. In some cases, the measurements were performed with ramping up and down H to confirm a hysteretic behavior (see the Supplemental Material [30]). At the lowest T of 0.49 K, $\rho(H)$ is zero in the field range of $\mu_0 H < 15$ T. Also, above ~15 T, a very small finite resistivity corresponding to the flux-flow resistivity seems to appear. However, it is observed just barely because the temperature is quite low relative to $T_c(H)$. The $\Delta\chi_{\rm ac}(H)$ exhibits several kinks [◇ marks in Fig. 3(a)]. In addition, minor step anomalies by small flux jumps are randomly observed [small arrows in Fig. 3(a)], along with a hysteretic behavior above $\mu_0 H_{\rm irr} \simeq 10.5$ T. Note that the kinks marked by ◇ in Fig. 3(a) appear in the same fields, despite this hysteresis, and that the ac response by a tiny rf field is sensitive to the vortex motion above $H_{\rm irr}$ (also see the Supplemental Material [30]).

At 1.0 K, the hysteretic behavior is observed in $\Delta\chi_{\rm ac}(H)$ above $\mu_0 H_{\rm irr} = 8.7$ T, suggesting a nonequilibrium depinning phase transition from a pinned vortex state to a mobile vortex state. As H increases above $\mu_0 H_{\rho\,\rm kink} = 13.6$ T, $\rho(H)$ becomes finite, then it saturates at $\mu_0 H_{\rho\rm kink} = 17$ T, as marked by Hourglass in Fig. 3(b). The finite $\rho(H)$ corresponds to the flux-flow resistivity described above. In contrast, at $T = 1.3$ K [Fig. 3(c)], as H increases from 5 T, the static vortex state in the LFSC phase suddenly collapses at $\mu_0 H = 13.3$ T and undergoes a transition completely to the normal state at $\mu_0 H = 14.1$ T. As H further increases, the onset of the HFSC state is observed at $\mu_0 H = 18.0$ T. Above this field, ρ decreases gradually and becomes almost constant above $\mu_0 H = 20.6$ T. This again corresponds to the flux-flow resistivity.

We summarize our experimental observations in $H \| b$ as the H–T phase diagram. In Fig. 4, we plot the characteristic temperatures and fields at which anomalies are observed in $\rho(T, H)$ and/or $\Delta\chi_{\rm ac}(T, H)$. We also show the color contour of $\rho(T, H)$ in the same figure to identify the region where the flux-flow resistivity appears. For the LFSC phase, the onset of $T_c = 2.1$ K at zero field is gradually suppressed by applying H and is continued to the kinks in ρ and $\Delta\chi_{\rm ac}$ in the SC state, labeled as (II) above $\mu_0 H^* \simeq 15$ T. Extrapolation of boundary (II) provides the upper critical field $H_{c2}^{\rm LFSC}(T \to 0)$ of the LFSC phase to be around 22 T.

On the other hand, the HFSC phase emerges above H^*, of which the boundary is labeled as (I) in Fig. 4. For $\rho(T)$ on the boundary (I), the detachment between the onset and kink temperatures becomes expanding from that in the LFSC transition. In addition, the kinks in $\Delta\chi_{\rm ac}$ are seen on both the high- and low-temperature side of $T_{\rho\,\rm kink}$. This broad feature of boundary (I) is consistent with the broad peak observed in the specific heat for the HFSC transition and the thermal expansion anomaly at T_c in the HFSC phase, which becomes blurred compared to that in the LFSC phase [19]. Remarkably, as shown in Fig. 4, the flux-flow resistivity is observed in a wide range of the HFSC phase below T_c, and zero resistivity appears only deep inside of the SC state [15,19]. Such a broadening of boundary (I) can be caused by flux motions due to SC fluctuations yielded in the high H.

The current study found an additional boundary called (III) (Fig. 4) that appears inside the LFSC phase. Boundary (III) is detected most clearly as the kink in $\Delta\chi_{\rm ac}$ from the H scan. Above ~ 0.7 K, it is also observable as $H_{\rho\,\rm kink}$, corresponding to the onset of flux-flow resistivity. As illustrated in Fig. 4, boundary (III) locates near H^* and is nearly T independent. Thus, this boundary is challenging to detect using specific heat or other thermodynamic probes with T scans. Recent specific heat measurement as a function of H [19] shows no obvious anomaly corresponding to boundary (III), suggesting that there may be no significant entropy change. Note that the flux-flow resistivity occurs between boundaries (II) and (III), while it is absent below boundary (III). Thus, the area between boundaries (II) and (III) is characterized by highly mobile vortices, similar to the HFSC phase. Boundary (III) may become noticeable because pinning centers have been significantly reduced in the high-quality crystal. Note that the boundary (III) does not coincide with $H_{\rm irr}$ where the hysterical behavior begins as denoted above as $\mu_0 H_{\rm irr}(0.49\ {\rm K}) = 10.5$ T and $\mu_0 H_{\rm irr}(1.0\ {\rm K}) = 8.7$ T (also see the Supplemental Material [30]).

Boundary (III) detected inside the LFSC phase near H^* indicates the possible existence of an intermediate SC

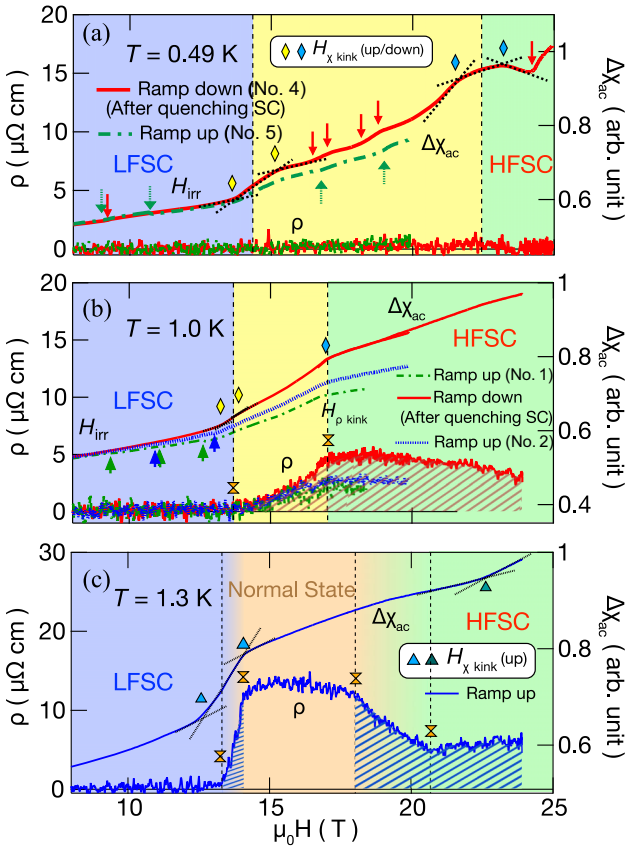

FIG. 3. Magnetic field dependence of ρ and $\Delta\chi_{ac}$ along the b axis for (a) $T = 0.49$ K, (b) $T = 1.0$ K, and (c) $T = 1.3$ K, respectively. The marks of diamond, triangle indicate the kink fields observed in both raising and lowering H and in the raising procedure, respectively. The symbol Hourglass represents the kink fields in ρ data. The colors of the symbols are the same as those of the symbols in Fig. 4. For $T = 0.49$ K, (i) H was lowered from 25 to 5 T after quenching the SC state by tilting the sample from the b axis and (ii) increased again to 20 T. For 1.0 K, (i) ramp up H from 5 to 18.5 T, (ii) quench the SC state by the sample rotation at 18.5 T, then ramp up H to 24 T, (iii) ramp down H_0 to 5 T, and finally (iv) ramp up again H to 20 T. The shaded hatch areas indicate areas where finite resistivity is observed. Small arrows indicate small steps of $\Delta\chi_{ac}$ due to small flux jumps.

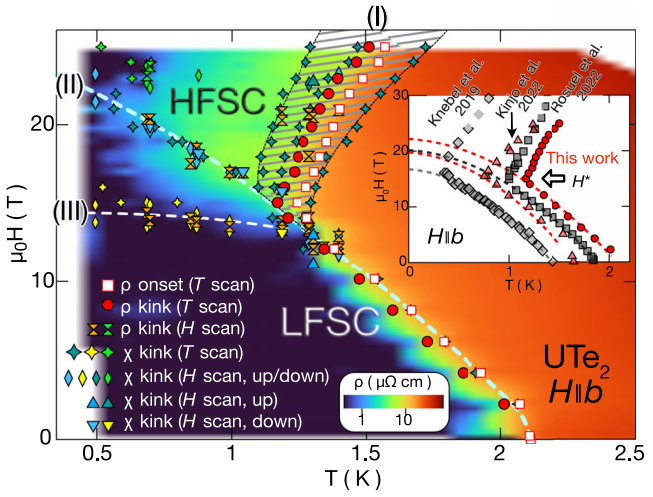

FIG. 4. H-T phase diagram for UTe_2 in the case of $H_0 \| b$. The colors of the symbols are the same as in Figs. 2 and 3. The symbol inverted triangle indicates the kink field observed in the procedure of lowering H. Color contour represents the electrical resistivity. The inset shows the comparison of $H_{c2}(T)$ for different T_c samples [15,19,20]. The dashed curves in the inset are eye guides for the minimal estimates of $H_{c2}^{\mathrm{LFSC}}(T \to 0)$.

phase characterized by a small flux pinning force between H^* and H_{c2}^{LFSC}. Thus, from the thermodynamic consideration [21], boundary (III) could be the missing transition line in the previously proposed phase diagram in UTe_2. However, whether this boundary is indeed connected to the intersection of the phase lines of boundaries (I) and (II) has not also been confirmed thus far. Whether the boundary (III) is an actual thermodynamic phase transition should also be confirmed.

The observation of boundary (III) also raises the possibility that the area between boundaries (II) and (III) can be regarded as a new intermediate phase, possibly emerging as a mixture of LFSC and HFSC states. Following a recent theoretical work [35], such a mixed state could be understood as the anapole SC phase if the LFSC and HFSC states might have different parity. The order parameters of the anapole SC phase are equivalent to an anapole (magnetic toroidal) moment and stabilize a nonuniform Fulde-Ferrell-Larkin-Ovchinnikov (FFLO) state. Highly mobile vortices with small currents might be expected in such an FFLO state. Furthermore, domain alignment by supercurrent may assist flux mobility. [35]. Alternatively, chiral SC symmetry proposed in UTe_2 [9–11,36] might also explain the vortex mobility by supercurrent because the directionality of SC pairing can form SC domains.

In the inset of Fig. 4, we compare $H_{c2}(T)$ in $H \| b$ reported for UTe_2 crystals with different qualities [15,19,20]. Evidently, quality improvement rapidly increases both the onset T_c and extrapolated $H_{c2}^{\mathrm{LFSC}}(0)$ (also see the Supplemental Material [30]). However, the characteristic field of $\mu_0 H^* \simeq 15$ T, above which the HFSC phase emerges on top of the LFSC phase, remains unchanged. This result might indicate that H^* is concerned with an internal electronic phase transition, such as a metamagnetic crossover or Lifshitz transition. In the case of $H \| a$, such a transition seems to boost the SC above 7 T [37]. However, in $H \| b$, no signature of the electronic transition was found in the normal state around 15 T. Because H^* is found to be independent of sample quality, the boundary (III), which branches off almost horizontally from H^*, most likely does not change its position much. Then, $H_{c2}^{\mathrm{LFSC}}(T)$ and the boundary (III) are probably too close to each other in the low-T_c samples to be detected separately.

In the last, we also note that the kink anomalies rest in the low-temperature high-H region above phase line (II)

shown as yellow-green-colored marks in Fig. 4. Further experiments at higher H are needed to investigate flux dynamics, as there is a possibility that the observed anomalies stem from vortex lattice melting and dynamics.

We thank M. Nagai and K. Shirasaki for their support in the experiments. We are also grateful for the stimulating discussions with K. Kubo, Y. Nagai, M. Machida, K. Ishida, H. Ikeda, K. Machida, and Y. Yanase. This work (a part of high magnetic field experiments) was performed at HFLSM under the IMR-Global Institute for Materials Research Tohoku (GIMRT) program (Proposals No. 202012-HMKPB-0012, No. 202112-HMKPB-0010, and No. 202112-RDKGE-0036). A part of this work was also supported by the Japan Society for the Promotion of Science (JSPS) KAKENHI Grants No. JP16KK0106, No. JP17K05522, No. JP17K05529, No. JP20K03852, No. JP20K03852, No. JP20H00130, No. JP20KK0061, No. JP20K20905, and No. JP22H04933 and by the JAEA REIMEI Research Program.

*sakai.hironori@jaea.go.jp

[1] S. Ran, C. Eckberg, Q.-P. Ding, Y. Furukawa, T. Metz, S. R. Saha, I.-L. Liu, M. Zic, H. Kim, J. Paglione, and N. P. Butch, Science **365**, 684 (2019).
[2] G. Nakamine, S. Kitagawa, K. Ishida, Y. Tokunaga, H. Sakai, S. Kambe, A. Nakamura, Y. Shimizu, Y. Homma, D. Li, F. Honda, and D. Aoki, J. Phys. Soc. Jpn. **88**, 113703 (2019).
[3] G. Nakamine, K. Kinjo, S. Kitagawa, K. Ishida, Y. Tokunaga, H. Sakai, S. Kambe, A. Nakamura, Y. Shimizu, Y. Homma, D. Li, F. Honda, and D. Aoki, Phys. Rev. B **103**, L100503 (2021).
[4] H. Fujibayashi, G. Nakamine, K. Kinjo, S. Kitagawa, K. Ishida, Y. Tokunaga, H. Sakai, S. Kambe, A. Nakamura, Y. Shimizu, Y. Homma, D. Li, F. Honda, and D. Aoki, J. Phys. Soc. Jpn. **91**, 043705 (2022).
[5] D. Braithwaite, M. Vališka, G. Knebel, G. Lapertot, J. P. Brison, A. Pourret, M. E. Zhitomirsky, J. Flouquet, F. Honda, and D. Aoki, Commun. Phys. **2**, 147 (2019).
[6] S. Ran, H. Kim, I. Lin Liu, S. R. Saha, I. Hayes, T. Metz, Y. S. Eo, J. Paglione, and N. P. Butch, Phys. Rev. B **101**, 140503(R) (2020).
[7] S. M. Thomas, F. B. Santos, M. H. Christensen, T. Asaba, F. Ronning, J. D. Thompson, E. D. Bauer, R. M. Fernandes, G. Fabbris, and P. F. S. Rosa, Sci. Adv. **6**, eabc8709 (2020).
[8] D. Aoki, F. Honda, G. Knebel, D. Braithwaite, A. Nakamura, D. Li, Y. Homma, Y. Shimizu, Y. J. Sato, J.-P. Brison, and J. Flouquet, J. Phys. Soc. Jpn. **89**, 053705 (2020).
[9] L. Jiao, S. Howard, S. Ran, Z. Wang, J. O. Rodriguez, M. Sigrist, Z. Wang, N. P. Butch, and V. Madhavan, Nature (London) **579**, 523 (2020).
[10] I. M. Hayes, D. S. Wei, T. Metz, J. Zhang, Y. S. Eo, S. Ran, S. R. Saha, J. Collini, N. P. Butch, D. F. Agterberg, A. Kapitulnik, and J. Paglione, Science **373**, 797 (2021).
[11] K. Ishihara, M. Roppongi, M. Kobayashi, Y. Mizukami, H. Sakai, Y. Haga, K. Hashimoto, and T. Shibauchi, arXiv:2105.13721.
[12] A. Haneveld and F. Jellinek, J. Less Common Metals **21**, 45 (1970).
[13] H. P. Beck and W. Dausch, Z. Naturforsch. B **43**, 1547 (1988).
[14] S. Ran, I.-L. Liu, Y. S. Eo, D. J. Campbell, P. M. Neves, W. T. Fuhrman, S. R. Saha, C. Eckberg, H. Kim, D. Graf, F. Balakirev, J. Singleton, J. Paglione, and N. P. Butch, Nat. Phys. **15**, 1250 (2019).
[15] G. Knebel, W. Knafo, A. Pourret, Q. Niu, M. Vališka, D. Braithwaite, G. Lapertot, M. Nardone, A. Zitouni, S. Mishra, I. Sheikin, G. Seyfarth, J.-P. Brison, D. Aoki, and J. Flouquet, J. Phys. Soc. Jpn. **88**, 063707 (2019).
[16] D. Aoki, A. Nakamura, F. Honda, D. Li, Y. Homma, Y. Shimizu, Y. J. Sato, G. Knebel, J.-P. Brison, A. Pourret, D. Braithwaite, G. Lapertot, Q. Niu, M. Vališka, H. Harima, and J. Flouquet, J. Phys. Soc. Jpn. **88**, 043702 (2019).
[17] A. Miyake, Y. Shimizu, Y. J. Sato, D. Li, A. Nakamura, Y. Homma, F. Honda, J. Flouquet, M. Tokunaga, and D. Aoki, J. Phys. Soc. Jpn. **88**, 063706 (2019).
[18] S. Imajo, Y. Kohama, A. Miyake, C. Dong, M. Tokunaga, J. Flouquet, K. Kindo, and D. Aoki, J. Phys. Soc. Jpn. **88**, 083705 (2019).
[19] A. Rosuel, C. Marcenat, G. Knebel, T. Klein, A. Pourret, N. Marquardt, Q. Niu, S. Rousseau, A. Demuer, G. Seyfarth, G. Lapertot, D. Aoki, D. Braithwaite, J. Flouquet, and J. P. Brison, Phys. Rev. X **13**, 011022 (2023).
[20] K. Kinjo, H. Fujibayashi, S. Kitagawa, K. Ishida, Y. Tokunaga, H. Sakai, S. Kambe, A. Nakamura, Y. Shimizu, Y. Homma, D. X. Li, F. Honda, D. Aoki, K. Hiraki, M. Kimata, and T. Sasaki, Phys. Rev. B **107**, L060502 (2023).
[21] S. K. Yip, T. Li, and P. Kumar, Phys. Rev. B **43**, 2742 (1991).
[22] L. P. Cairns, C. R. Stevens, C. D. O'Neill, and A. Huxley, J. Phys. Condens. Matter **32**, 415602 (2020).
[23] P. F. S. Rosa, A. Weiland, S. S. Fender, B. L. Scott, F. Ronning, J. D. Thompson, E. D. Bauer, and S. M. Thomas, Commun. Mater. **3**, 33 (2022).
[24] Y. Haga, P. Opletal, Y. Tokiwa, E. Yamamoto, Y. Tokunaga, S. Kambe, and H. Sakai, J. Phys. Condens. Matter **34**, 175601 (2022).
[25] A. Weiland, S. M. Thomas, and P. F. S. Rosa, JPhys. Mater. **5**, 044001 (2022).
[26] H. Sakai, P. Opletal, Y. Tokiwa, E. Yamamoto, Y. Tokunaga, S. Kambe, and Y. Haga, Phys. Rev. Mater. **6**, 073401 (2022).
[27] D. Aoki, H. Sakai, P. Opletal, Y. Tokiwa, J. Ishizuka, Y. Yanase, H. Harima, A. Nakamura, D. Li, Y. Homma, Y. Shimizu, G. Knebel, J. Flouquet, and Y. Haga, J. Phys. Soc. Jpn. **91**, 083704 (2022).
[28] A. G. Eaton, T. I. Weinberger, N. J. M. Popiel, Z. Wu, A. J. Hickey, A. Cabala, J. Pospisil, J. Prokleska, T. Haidamak, G. Bastien, P. Opletal, H. Sakai, Y. Haga, R. Nowell, S. M. Benjamin, V. Sechovsky, G. G. Lonzarich, F. M. Grosche, and M. Valiska, arXiv:2302.04758.
[29] C. Broyles, Z. Rehfuss, H. Siddiquee, K. Zheng, Y. Le, M. Nikolo, D. Graf, J. Singleton, and S. Ran, arXiv:2303.09050.

[30] See Supplemental Material at http://link.aps.org/supplemental/10.1103/PhysRevLett.130.196002 for (i) magnetic field orientation dependence of ρ and $\Delta\chi_{ac}$, (ii) T dependence of ρ at various H, (iii) T dependence of $\Delta\chi_{ac}$ at various H, (iv) close look of $\Delta\chi_{ac}(H)$, and (v) comparison with previously reported sc H-T phase diagram along the b axis in UTe_2.

[31] D. Aoki, T. D. Matsuda, V. Taufour, E. Hassinger, G. Knebel, and J. Flouquet, J. Phys. Soc. Jpn. **78**, 113709 (2009).

[32] F. Lévy, I. Sheikin, B. Grenier, C. Marcenat, and A. Huxley, J. Phys. Condens. Matter **21**, 164211 (2009).

[33] T. Hattori, Y. Ihara, Y. Nakai, K. Ishida, Y. Tada, S. Fujimoto, N. Kawakami, E. Osaki, K. Deguchi, N. K. Sato, and I. Satoh, Phys. Rev. Lett. **108**, 066403 (2012).

[34] Y. Tokunaga, D. Aoki, H. Mayaffre, S. Krämer, M.-H. Julien, C. Berthier, M. Horvatić, H. Sakai, S. Kambe, and S. Araki, Phys. Rev. Lett. **114**, 216401 (2015).

[35] S. Kanasugi and Y. Yanase, Commun. Phys. **5**, 39 (2022).

[36] S. Bae, H. Kim, Y. S. Eo, S. Ran, I.-l. Liu, W. T. Fuhrman, J. Paglione, N. P. Butch, and S. M. Anlage, Nat. Commun. **12**, 2644 (2021).

[37] Y. Tokiwa, P. Opletal, H. Sakai, K. Kubo, E. Yamamoto, S. Kambe, M. Kimata, S. Awaji, T. Sasaki, D. Aoki, Y. Tokunaga, and Y. Haga, arXiv:2210.11769.